Journal of Environmental Chemical Engineering 9 (2021) 105239

Contents lists available at ScienceDirect

Journal of Environmental Chemical Engineering

journal homepage: www.elsevier.com/locate/jece

Glycerol purification using reactivated spent bleaching earth from palm oil refineries: Zero-waste approach

Maria Yuliana [a,*], Luciana Trisna [b], Feprita Sari [b], Valentino Bervia Lunardi [a]

[a] Department of Chemical Engineering, Widya Mandala Surabaya Catholic University, Kalijudan 37, Surabaya 60114, Indonesia
[b] Department of Quality Assurance and Product Development, PT. Batara Elok Semesta Terpadu, Maspion Industrial Estate, Gamma Q-2, Gresik 61151, Indonesia

ARTICLE INFO

Editor: Dr. GL Dotto

Keywords:
Reactivated spent bleaching earth
Surfactant intercalation
Glycerol purification
Mechanism study
Isotherm study
Zero-waste approach

ABSTRACT

This work uses reactivated spent bleaching earth (RSE) from palm oil refineries to reduce the impurities content (e.g., free fatty acid (FFA), carotenoid and chlorophyll) in crude glycerol. The influences of three important reactivation parameters on the removal of impurities are studied. The maximum removal percentage of all impurities is obtained using the RSE fabricated at activation temperature $T = 40$ °C, n-hexane to spent earth ratio $m_h = 15$, and surfactant loading $m_c = 0.75$ wt%; which, hereinafter referred to as RSE-m. Further glycerol purification test using RSE-m at various adsorption temperature (T_a) and RSE-m loading (m_a) show that FFA, carotenoid, and chlorophyll are effectively reduced by 47.45, 93.39, and 96.63 wt%, respectively, at $T_a = 50$ °C and $m_a = 10$ wt%., with all specification comparable, if not superior, to those of commercial industrial grade glycerol. The kinetic, isotherm and thermodynamic studies also suggest that the adsorption of the pigmented compounds on the RSE-m surface is spontaneous, endothermic, and driven by physical attraction via hydrophobic binding (for both pigments) and electrostatic interaction (for chlorophyll only). The adsorption results indicate that RSE-m has a great affinity to all glycerol impurities, and can be considered as a promising adsorbent for glycerol purification. As this study implements the zero-waste approach by using RSE, it will prominently reduce the solid waste generated by the palm oil refineries, and at the same time, offers a cost-effective route for the refining of glycerol.

1. Introduction

The substantial increase in biodiesel production in the last decade results in a significant increase in crude glycerol production. Monteiro et al. (2018) stated that global biodiesel production is predicted to increase 4.5% annually, and reach 41 million kiloliters in the next two years [1]. According to the Indonesian Directorate General of Renewable Energy and Every Conservation, the country produces more than 9 million kiloliters of biodiesel in 2020 [2]. In all cases, the production of biodiesel produces two phases: (1) the upper phase containing biodiesel, and (2) the lower phase consisting of crude glycerol with the purity of 50–90 wt%, excess methanol, water, salts, and other by-products [3]. The latter represents 10–12 wt% of the total biodiesel product [4,5].

Being the major by-product in biodiesel production, the recent market price of crude glycerol is only US$ 0.08 – 0.18 per kilogram; while pure glycerol (>99% purity) costs around US$ 0.70–1.96 per kilogram [6]. This significant market value difference is basically due to the presence of impurities in the crude glycerol which limits its conversion to a higher-value product and industrial use. Improving the purity of glycerol requires several processing steps, including neutralization, sedimentation, distillation, and bleaching/purification using activated carbon; therefore, the market price of pure glycerol is observed to be ten-folds higher than that of crude glycerol. While crude glycerol may be used as an improver of wastewater sludge performance [7], high purity glycerol has found wider use in various industries, ranging from polymer, pharmaceutical, cosmetics to food products [6].

The bleaching procedure is regarded as the most important step in glycerol purification as this step significantly reduces the bulk pigmented compounds (e.g., carotenoids and chlorophyll), odor, and free fatty acids (FFA) contained in the crude glycerol. Currently, many industries and engineering companies use activated carbon (AC) as the bleaching agent for the purification of glycerol [8,9]. AC possesses a high adsorption capacity compared with the other adsorbents. However, although AC is an excellent adsorbent, it is also expensive for adsorption. Therefore, several types of research have been conducted to replace the use of AC with other minerals, including montmorillonite [10] and

* Corresponding author.
E-mail addresses: mariayuliana@ukwms.ac.id, maria_yuliana_liauw@yahoo.com (M. Yuliana).

https://doi.org/10.1016/j.jece.2021.105239
Received 20 January 2021; Received in revised form 9 February 2021; Accepted 15 February 2021
Available online 18 February 2021

Table 1
The specification of the crude glycerol.

Properties	Unit	Results
Glycerol content	wt%	96.79
Color	–	190 (Pt-Co)
Moisture	wt%	1.62
pH	–	6.9
Ash	wt%	0.10
Salt content	ppm	17
FFA content	wt%	1.37
Carotenoids content	ppm	12.11
Chlorophyll content	ppm	0.89

organobentonites [11].

Currently, Indonesia produces almost 40 million tons of crude palm oil every year [12], with around 1.0–1.2 million tons of bleaching earth utilized for purification. Approximately 200,000 – 300,000 tons of oil are carried over along with this bleaching agent [13], generating around 1.2–1.5 million tons of spent earth (SE) annually which, in Indonesia, is often directly discharged to the environment as solid waste. With the enormous amount, SE can be an abundant raw material to prepare waste-based adsorbent. This study aims to implement the zero-waste approach by replacing AC with SE from the palm oil refineries in the glycerol purification. It will prominently reduce solid waste, and at the same time, offers a cost-effective route for the refining of glycerol.

The SE reactivation will be performed via solvent washing and surfactant intercalation. Currently, the chemical-intercalated materials have attracted wide attention, specifically in adsorption-related studies. Zhu et al. (2019) and Zhu et al. (2020) employ the use of L-lysine modified montmorillonite and amino trimethylene phosphonic acid-intercalated layered double hydroxide to improve the removal rate of heavy metals (Cu^{2+} and Pb^{2+}) [14,15], while Santoso et al. (2020) use rarasaponin-intercalated bentonite to adsorb β-carotene from the palm oil [16]. In this study, three independent parameters to restore the adsorption capability of SE, including the different mass ratio of hexane to SE m_h, surfactant loading m_c, and activation temperature T will be investigated. The performance of glycerol purification using the reactivated SE (RSE) at various reactivation variables is evaluated by the removal of each impurity, i.e., FFA, carotenoid, and chlorophyll content. The adsorption behavior of the pigmented compounds onto the RSE surface is also observed through the kinetic, isotherm, thermodynamic studies.

2. Materials and methods

2.1. Materials

Sample of SE and palm-based crude glycerol were supplied by a local palm oil manufacturer in Indonesia. While SE was collected from their edible oil refinery plant, the crude glycerol was obtained from their biodiesel process. The crude glycerol has already undergone three initial purification steps, e.g., neutralization, sedimentation, and distillation processes. The technical specification of the crude glycerol used in this study is presented in Table 1. All chemicals and reagents purchased from Merck and Sigma-Aldrich (Germany) were of analytical grade and do not require further purification.

2.2. Reactivation of SE

Initially, n-hexane and SE with various mass ratios (m_h = 5, 10, 15) were mixed under a constant agitation of 300 rpm at 40 °C for 30 min. The mixture was centrifuged at 4500 rpm for 30 min to separate the deoiled SE from the supernatant. The solid was then dried in an oven at 100 °C for 60 min to remove the retained hexane. The calcination of the deoiled SE was conducted in a muffle furnace at 550 °C for 120 min to obtain calcined SE. The surface activation of SE was performed by inserting cetyltrimethylammonium bromide (CTAB) into the silanol layer of SE. A certain amount of SE was dispersed in the CTAB/water mixture with various surfactant concentrations ranging from m_c = 0.5–1.0 wt%. The activation was conducted at three different temperatures (T = 30, 40, 50 °C) for 180 min. The solid was filtered through Whatman no.1 under vacuum and water-washed repeatedly. The surfactant-activated SE was then dried at 120 °C and pulverized to a 100–150 μm particle size. The resulting material was denominated as RSE.

2.3. The performance of RSE obtained at various reactivation conditions in the glycerol purification

To determine the performance of every RSE sample obtained at various reactivation conditions, a mixture of crude glycerol and 3 wt% of RSE was stirred (300 rpm) at 30 °C for 60 min. After adsorption, the glycerol was collected for FFA, carotenoids, and chlorophyll analysis. The content of the three impurities was determined following the standard method of AOCS Ca 5a-40, MPOB 2005 [17,18], and AOCS Cc 13d-55. The removal rate of each impurity (in wt%) was calculated using the equation below:

$$\text{Impurities removal(wt\%)} = 100\left(\frac{C_0 - C_f}{C_0}\right) \quad (1)$$

where C_0 and C_f correspond to the initial and final impurities concentration in wt% for FFA and ppm for both pigmented compounds, respectively. The RSE sample obtained at the reactivation condition which gives the highest impurities removal rate will be, hereinafter, written as RSE-m.

2.4. The influence of adsorption temperature and RSE loading on the removal rate of FFA, carotenoids, and chlorophyll

Various RSE-m to crude glycerol mass ratios (m_a = 1–10 wt%) were subjected to a 60-min adsorption process at constant temperature and stirring rate (300 rpm). The determination of adsorption time was based on the adsorption kinetic study (Section 2.6). Three adsorption temperatures (T_a = 30, 50, 70 °C) were employed to study the influence of temperature on the removal of FFA, carotenoids, and chlorophyll. The spent RSE-m is regenerated by calcination at 550 °C, followed by the steps described in Section 2.2, for recyclability study. Meanwhile, the content analysis of the three impurities after adsorption and the calculation of the removal rate were performed using the same procedures mentioned in Section 2.3.

2.5. Recyclability of RSE-m

RSE-m was repeatedly used for the 5 cycles of the adsorption process at the condition where the maximum removal of glycerol impurities was obtained. The recyclability of RSE-m was determined by the number of repetitions until when the removal rate of impurities became significantly lower than the initial use. All experiments were carried out in triplicates to verify the results.

2.6. Adsorption kinetics, isotherm, and thermodynamic studies of pigmented compounds

The adsorption kinetics was used to determine the equilibrium time for the adsorption of pigmented compounds onto RSE-m. Briefly, glycerol was introduced into a series of beaker glass. Subsequently, RSE-m (m_a = 10 wt%) was added into the glass and stirred to keep the system homogenous. This study was conducted at T_a = 50 °C. At a specific interval of time, one beaker glass was taken to measure the loaded amount of pigments in RSE-m.

Meanwhile, the adsorption isotherm study was employed using the

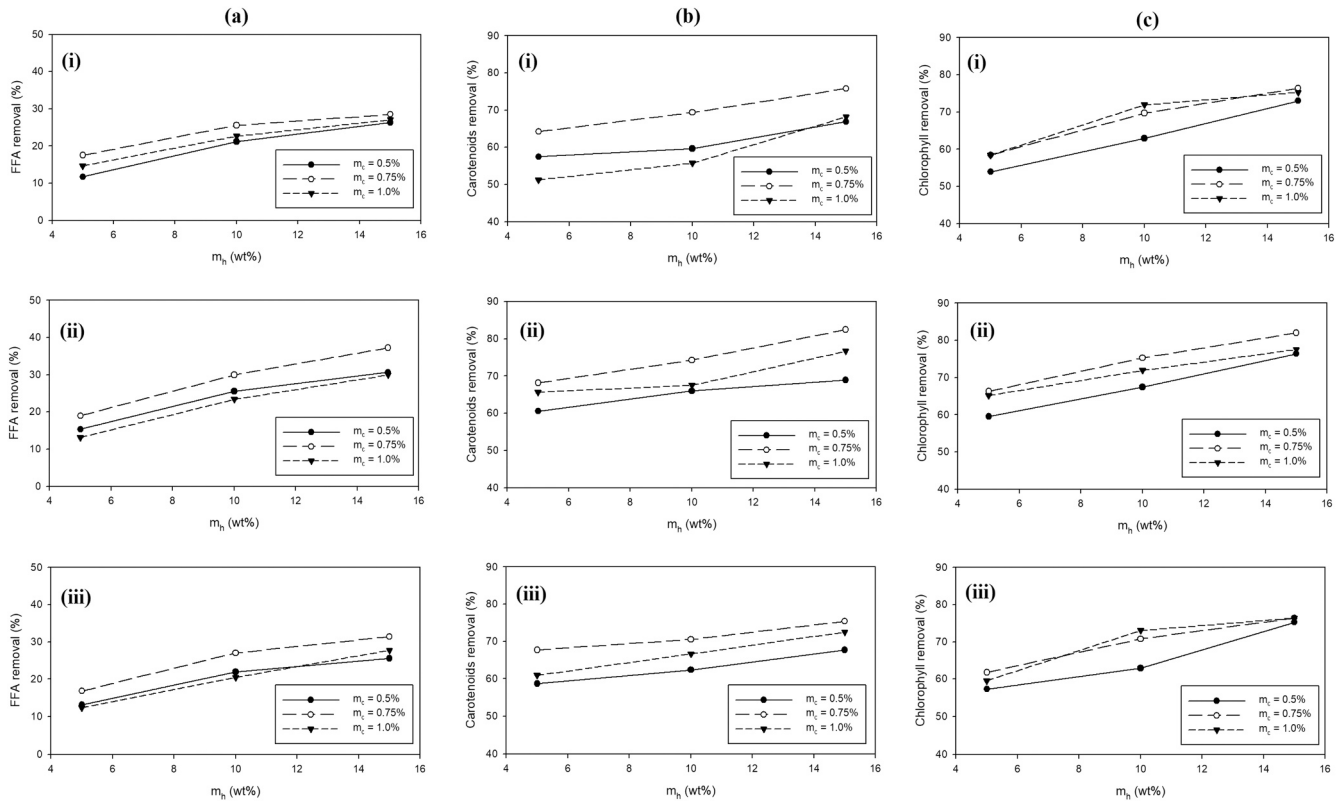

Fig. 1. The removal rate of (a) FFA, (b) carotenoids, (c) chlorophyll varied with CTAB loading at (i) $T = 30$ °C, (ii) $T = 40$ °C, (iii) $T = 50$ °C.

adsorption data obtained from Section 2.4. The equilibrium mass of adsorbed pigments per unit mass of RSE-m can be expressed as

$$Q_e(\mathrm{mg/g}) = V\left(\frac{C_i - C_e}{m_a}\right) \tag{2}$$

where C_i and C_e correspond to the initial and equilibrium concentrations of pigments in glycerol (mg/L), m_a is the loaded RSE-m (g), and V is the volume of glycerol (L). The data obtained at the equilibrium condition were then fitted to Langmuir, Freundlich, Dubinin-Radushkevich (D-R) isotherms. The obtained isotherm parameters were further analyzed to determine Gibbs free energy (ΔG°), enthalpy (ΔH°), entropy (ΔS°).

2.7. Characterization of the optimized RSE (RSE-Opt)

The scanning electron microscopy (SEM) images of RSE-m were captured using JEOL JSM-6500 F (Jeol Ltd., Japan) with 10 kV accelerating voltage and a 8.0 mm working distance, while its specific surface area and pore volume were determined at 77 K using a Micromeritics ASAP 2010 sorption analyzer. The surface functional groups of RSE-m were determined using Shimadzu FTIR 8400 s at 4000–40 cm^{-1}. The point-of-zero-charge (pH_{pzc}) of RSE-m is determined by Malvern Zetasizer Nano Z (Malvern Panalytical Ltd., United Kingdom) from the pH of 2–11.

3. Results and discussions

3.1. The influence of reactivation variables on the performance of RSE

Fig. 1 shows the influence of three independent variables (T, m_h, m_c) on the removal rate of FFA (Fig. 1a), carotenoids (Fig. 1b), and chlorophylls (Fig. 1c). Notably, the CTAB loading at $m_c = 0.75\%$ gives the highest removal rate for all three glycerol impurities. A better removal rate can be attributed to the enlargement of basal spacing in the interlayer of clay due to the intercalation of CTAB. As the impurities (i.e., FFA, carotenoids, and chlorophyll) are hydrophobic, easier migratory movement onto the interlayer region also provokes the hydrophobic binding between FFA, pigmented components, and hydrophobic tail of CTAB in RSE. Meanwhile, further increasing the amount of CTAB causes the saturation in the RSE surface, caused by the formation of admicellar region between the tail of intercalated CTAB and the tail of the free surfactant ions [19,20]. This lowers the number of active sites available for the adsorption of the impurities in crude glycerol, hence, decreasing the removal rate.

A similar trend is also observed for the intercalation temperature, where the removal of FFA, carotenoids, and chlorophyll moderately escalate along with the temperature from $T = 30$ °C to $T = 40$ °C. A higher temperature induces the dissolution of surface cations from the surface of RSE, which leaves RSE in a negative and unstable state. This urges the cationic head of CTAB to associate with the surface and stabilize its charge [21]. This creates a hydrophobic region that is favorable for the adsorption of the hydrophobic compounds, including FFA, carotenoids, and chlorophyll. However, as seen in Fig. 1, increasing the intercalation temperature further to $T = 50$ °C declines the rate slightly. A higher amount of cationic CTAB linked onto the surface of RSE forms a denser region filled with hydrophobic tails in the interlayer spacing, which consequently covers the binding area of RSE and lowers down its ability to interact with the impurities.

As depicted in Fig. 1, the mass ratio of n-hexane to SE in the washing procedure has a significant influence on the removal of all glycerol impurities. With the increase of n-hexane to RSE mass ratio from $m_h = 5$ to $m_h = 15$ in the regeneration of RSE, the removal percentage of FFA was observed to have amplified by 1.5 folds, while it was 1.2–1.3 folds for the pigmented compounds. A greater mass ratio of n-hexane to SE results in a forthright migration of the attached organic compounds in the surface of SE to n-hexane, which leaves higher active sites in RSE and therefore, leads to a higher removal rate of impurities [22,23].

Based on the experimental results, the reactivation condition to achieve the highest removal rate of FFA, carotenoids, and chlorophyll is

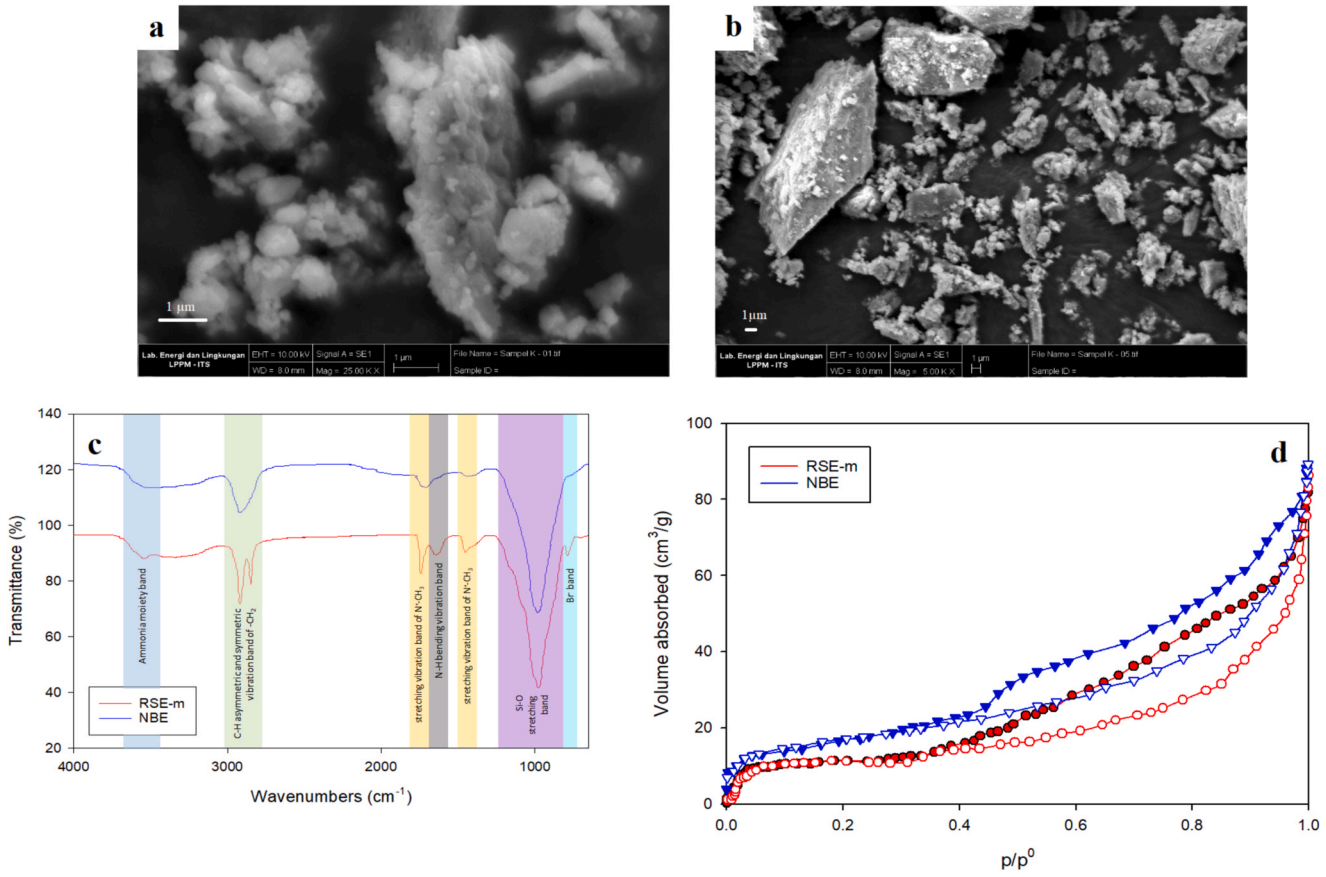

Fig. 2. (a) – (b) The SEM images of RSE-m and NBE, (c) FTIR spectra, (d) N_2 sorption isotherm profiles of RSE-m and NBE. (For interpretation of the references to colour in this figure, the reader is referred to the web version of this article.)

Table 2
The textural properties of RSE-m and NBE.

Materials	S_{BET} (m^2/g)	V_p (cm^3/g)
RSE-m	73.1	0.164
NBE	67.4	0.107

monitored at $T = 40$ °C, $m_h = 15$, and $m_c = 0.75$ wt%. The low temperature ($T = 40$ °C) and CTAB loading (0.75 wt%) are generally favorable in the industries as the low value of these two factors directly provide a positive contribution to the production efficiency.

3.2. Characteristics of RSE-m

Fig. 2a–b shows the respective surface topographies of RSE-m and fresh bleaching earth (NBE). The morphologies of the prepared RSE-m and NBE are observed to be similar, implying that the reactivation procedures do not change their macrostructure. A consistent result is also seen from the microscopic viewpoint, where based on their nitrogen sorption profiles (Fig. 2d), the pore structure of both bleaching earth shares the same type I isotherm with an H3-type hysteresis loop. This profile indicates that the minerals are composed of microporous, non-uniform, and very complex pore structure, with slit/plane shapes [24]. Meanwhile, the textural properties of RSE-m and NBE are presented in Table 2 where RSE-m possesses comparable, if not superior, properties to NBE. This may be contributed to the expansion of the interlayer spacing due to the CTAB intercalation [25,26], which is one of the reactivation procedures.

The N_2-sorption result agrees well with the FTIR spectra depicted in Fig. 2c (red line), which observes several specific functional groups of

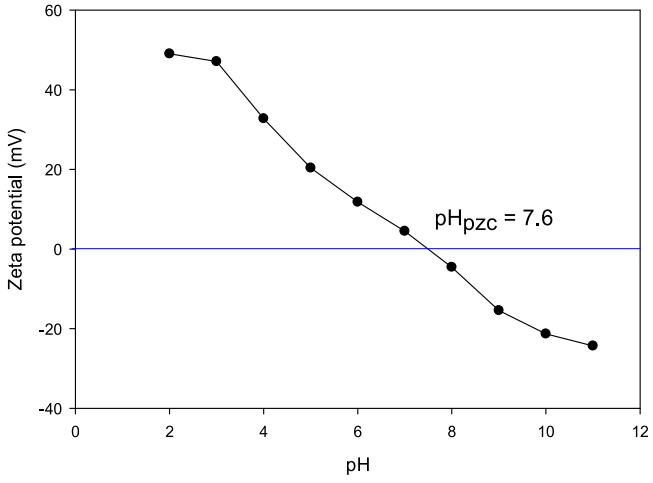

Fig. 3. Determination of pH at point-of zero-charge (pH_{pzc}) of RSE-m.

CTAB, e.g., the ammonia moiety band (3386 cm^{-1}), C–H asymmetric and symmetric vibration bands of $–CH_2$ (2930–2852 cm^{-1}), stretching vibration band of N^+-CH_3 (1652 cm^{-1} and 1467 cm^{-1}), N-H bending vibration band at 1570 cm^{-1}, and Br^- band (732 cm^{-1}), suggesting that CTAB has been intercalated into the lamellar spacing of RSE-m. Fig. 3 shows that the pH_{pzc} of RSE-m is observed at 7.6. As the impurities adsorption from glycerol happens at neutral pH (its natural pH), the RSE-m surface will be positively charged (adsorption pH < pH_{pzc}) during the runs [27].

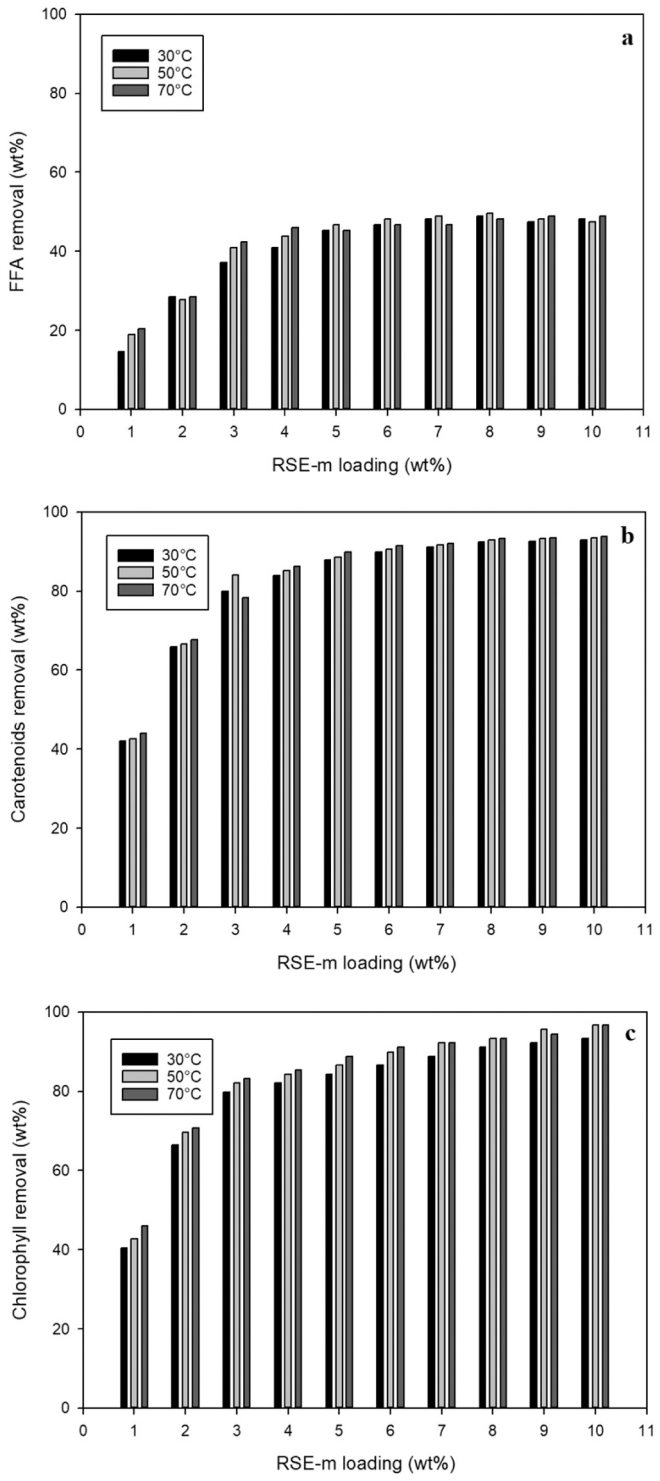

Fig. 4. The removal rate of (a) FFA, (b) carotenoids, (c) chlorophyll varied with the loading of RSE-m at various temperature.

3.3. Adsorption of the glycerol impurities using RSE-m

Fig. 4 presents the removal rate of FFA, carotenoids, and chlorophyll at the various temperature T_a and RSE-m loading m_a. The removal percentage of all three impurities is monitored to enhance along with the RSE-m loading from $m_a = 1$ wt% to $m_a = 10$ wt% in all tested temperatures, with an exponential increase observed in the first half. The results indicate that the impurities removal is proportional to the number of binding sites offered by RSE-m. It also shows that RSE-m possesses a good dispersion ability in crude glycerol, where the amount of RSE-m does not influence the diffusion path length for the impurities to migrate from the bulk region onto the RSE-m surface [28]. Meanwhile, the adsorption temperature also influences the impurities reduction rate in crude glycerol. Notably, increasing the temperature from $T = 30$ °C to $T = 50$ °C improves the removal rate of all impurities. Escalating the adsorption temperature lowers the solution viscosity, and at the same time, enhances the kinetic energy and mobility of the adsorbate [29]. This causes the particle collision to intensify, and therefore, it is easier to achieve the activation energy of the adsorption. However, increasing the adsorption temperature further to $T = 70$ °C shows an irregular trend of adsorption rate, where at some points, the impurities removal rates are higher, while at the others lower. Although higher temperature increases the diffusion rate of adsorbate, More (2018) stated that excessive collision of particles, on the other hand, tends to remove the adsorbate from the adsorbent; therefore, this fluctuating phenomenon happens after a certain temperature [30]. Based on the results, the maximum removal of the three impurities is obtained at the adsorption condition of $T = 50$ °C, $t = 60$ min, and $m_a = 10$ wt%. The properties of the glycerol after adsorption are presented in Table 3. The analysis results indicate that the resulting glycerol has similar specifications to the commercial industrial-grade glycerol. Table 4 also shows the comparison study of glycerol purification using various types of adsorbent, including RSE-m. In general, RSE-m has comparable adsorption capacity towards glycerol impurities, e.g., FFA and pigmented compounds, with the other adsorbents reported in the literature, as evident from the clear color obtained in this study.

Table 3
The properties of the resulting glycerol after adsorption ($T_a = 50$ °C, $t = 60$ min, and $m_a = 10$ wt%).

Properties	Unit	Resulting glycerol	Industrial grade glycerol [31]
Glycerol content	wt%	98.67	98 min
Color	Pt/Co	34	40 max
Moisture	wt%	0.42	2.0 max
pH	–	7.1	–
Ash	wt%	0.08	–
Salt content	ppm	8	10 ppm max
FFA content	wt%	0.69	1.0 max
Carotenoids content	ppm	0.80	–
Chlorophyll content	ppm	0.03	–

The recyclability of RSE-m is evaluated for five adsorption and regeneration cycles, with the results presented in Fig. 5. The results indicate that RSE-m can maintain a high removal rate of glycerol impurities until the fourth cycle, before moderately decreases at the fifth cycle. The loss of adsorption capacity is likely attributed to the less available active sites in the regenerated adsorbent, caused by the incomplete removal of impurities from the clay structure. A similar performance has been reported for saponin-intercalated bentonite where four cycles seem to be an average number in terms of its recyclability [16].

3.4. Adsorption kinetics, isotherm, and thermodynamic studies of the pigmented compounds

The adsorption kinetics of carotenoids and chlorophylls with RSE-m as the host is studied to find the equilibrium adsorption time and represented by the pseudo-first-order (Eq. 3) and pseudo-second-order (Eq. 4) equations below.

$$Q_t = Q_e(1 - e^{-k_1 t}) \quad (3)$$

$$Q_t = \frac{Q_e^2 k_2 t}{(1 + Q_e k_2 t)} \quad (4)$$

Table 4
The adsorption ability of various adsorbents for glycerol purification.

Adsorbent type	Adsorption condition	Removal rate (wt%)			Color	Reference
		FFA	Carotenoids	Chlorophyll		
HDTMA-modified bentonite	$T_a = 50$ °C, $m_a = 1$ wt%, $t = 60$ min	N/A	50.6	50.8	Light brown	[11]
Reactivated spent AC	$T_a = 30$ °C, $m_a = 1$ wt%, $t = 60$ min	38.64	40.0	64.29	Light brown	[18]
Sludge derived-AC	$T_a = 30$ °C, $m_a = 5.3$ wt%, $t = 120$ min	N/A	N/A	N/A	Yellow (2314 ± 141, Pt–Co unit)	[32]
RSE-m	$T_a = 50$ °C, $m_a = 10$ wt%, $t = 60$ min	47.45	93.39	96.63	Clear (34, Pt–Co unit)	This work

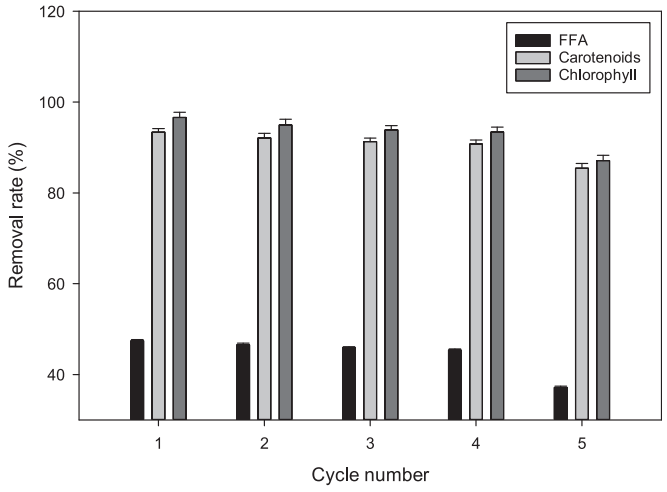

Fig. 5. Recyclability of RSE-m in the adsorption of glycerol impurities.

where Q_e and Q_t (mg/g) represent the corresponding amount of pigments adsorbed on RSE-m at equilibrium and at adsorption time t (min), k_1 and k_2 are the adsorption constants for pseudo-first-order and pseudo-second-order kinetics, respectively. Fig. 6 presents the adsorption kinetic curves built from the experimental data, with the adsorption equilibrium time observed at 60 min, while the calculated parameters are given in Table 5. As indicated by the value of the coefficient of determination (R^2), the fitted adsorption kinetic curves point that the pseudo-first-order equation can represent the calculated and experimental data better than that of pseudo-second-order, implying that the physisorption controls the adsorption more than chemisorption. The value of k_1 which is higher than k_2 indicates that the intra-particle diffusion is the rate-limiting step in the adsorption of pigments onto RSE-m [33,34].

The equilibrium data (Section 3.3) at three different temperatures are fitted into several isotherm equations, e.g., Langmuir, Freundlich, and D-R isotherms (Table 6). Fig. 7 shows the fitted isotherms of the equilibrium data of the pigmented compounds adsorption at $T_a = 50$ °C. Using the nonlinear curve fitting, the value of 1/n is obtained at the range of 0.59–0.62 for carotenoids, and 0.61–0.65 for chlorophyll, indicating that the adsorption of both pigmented components is favorable [35]. Aside from the lower value observed at 70 °C in the adsorption of carotenoids, the increasing value of the Freundlich constant (K_F) along with the temperature for both carotenoids and chlorophyll suggests that the pigment adsorption on the RSE-m surface is endothermic. (Table 7)

A similar trend is also observed when the Langmuir model is applied. An increase of the Langmuir constant (K_L) from 0.17 L/mg to 0.20 L/mg for carotenoids, and from 1.85 L/mg to 2.61 L/mg for chlorophyll as the temperature escalates from $T_a = 30$ °C to $T_a = 70$ °C, implying that the adsorption favors high temperature, and is indeed endothermic. The computed $Q_{m(L)}$ is monitored to be enhanced from 804.69 mg/g at $T_a = 30$ °C to 850.51 mg/g at $T_a = 50$ °C, before slightly declines to 844.80 mg/g at $T_a = 70$ °C for carotenoids. Meanwhile, the value of $Q_{m(L)}$ in the adsorption of chlorophyll is found to gradually increase from 64.04 mg/g to 67.70 mg/g as the temperature increase from the lowest to the highest point. To evaluate the mechanism of the pigmented compounds adsorption onto the RSE-m, the D-R isotherm model is employed. Mean sorption energy (E) can be calculated using the equation below:

$$E = \frac{1}{\sqrt{2\beta}} \quad (5)$$

where E and β have a unit of kJ/mol and $mmol^2/J^2$, respectively. An E value with a range of 8–16 kJ/mol points that the sorption is governed by chemical binding, while the E value lower than 8 kJ/mol suggests that the sorption occurs via physical interaction [29,36,37]. Table 4 shows that all E values in the tested range are lower than 8 kJ/mol, indicating that the adsorption mechanism of both pigmented compounds is governed by physical binding.

The thermodynamic parameters, e.g., Gibbs free energy change (ΔG°), enthalpy (ΔH°), and entropy (ΔS°) are determined, and the results are summarized in Table 7. The Gibbs free energy (ΔG°) values for all adsorption temperatures are found to be negative, implying spontaneous and favorable adsorption of pigmented compounds. The increasing magnitude of ΔG° alongside the temperature concludes that the higher affinity of both compounds on the RSE-m is achieved by escalating the temperature. These results agree well with the positive enthalpy value found in the adsorption of carotenoids and chlorophyll (3.399 kJ/mol and 7.336 kJ/mol, respectively), which confirms the endothermic nature of the adsorption process. The corresponding values of ΔS° for carotenoids and chlorophyll adsorption are observed at 106.5 J/mol.K and 143.6 J/mol.K, reflecting the increased randomness at the solid-liquid interface at the higher temperature, which leads to the enhanced affinity of the adsorbate (pigmented compounds) to the adsorbent (RSE-m) [38].

3.5. The adsorption behavior and mechanism of RSE

The interaction between the glycerol impurities, specifically the pigmented compounds, and the surface of RSE-m is depicted based on three important points: (1) the surface properties of adsorbent, (2) the structure of adsorbate, and (3) the results of the adsorption kinetics, isotherms, and thermodynamics studies. The RSE-m particle is constructed by the negative charge bentonite, attapulgite, and sepiolite [39–41], with the surface covered by the cationic head of CTAB to form a hydrophobic adsorbent with wider lamellar spacing. During the adsorption process, the surface of RSE-m is supposed to have a positive charge because the adsorption runs at neutral pH, which is lower than the pH_{pzc} of RSE-m. Meanwhile, as a fat-soluble pigment, both carotenoids, and chlorophyll exhibit extreme hydrophobicity. Chlorophyll is also known to have a basic structure comprising the negatively charged porphyrin ring which is coordinated to a central magnesium atom.

Based on the findings of the study, the adsorption of carotenoids is mainly governed by the physical hydrophobic attraction, while the adsorption of chlorophyll is driven by both electrostatic interaction (due to the opposite charge of chlorophyll and RSE-m during the adsorption) and hydrophobic binding. The mechanism steps of the pigmented

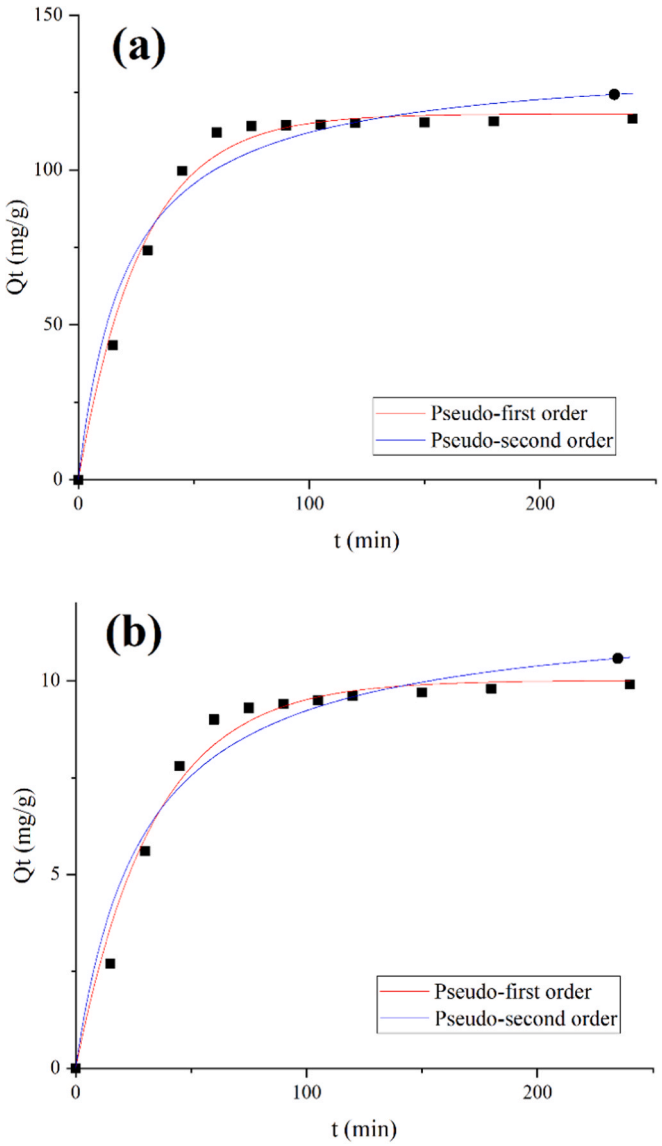

Fig. 6. Adsorption kinetic curves for the adsorption of (a) carotenoids and (b) chlorophyll onto RSE-m.

Table 5
The kinetics parameters of the adsorption of pigmented compounds onto RSE-m surface.

Model	Parameters	Pigmented compounds	
		Carotenoids	Chlorophyll
Pseudo-first order	k_1 (g/mg.min)	0.037	0.030
	Qe (mg/g)	118.12	10.01
	R^2	0.9893	0.9848
Pseudo-second order	k_2 (g/mg.min)	0.0004	0.003
	Q_e (mg/g)	135.70	11.87
	R^2	0.9611	0.9585

compounds onto the surface of RSE-m may be assumed to follow the points below:

- Migration of carotenoids and chlorophyll from the bulk region of glycerol to the boundary layer of RSE-m
- As the retained water molecules in glycerol and RSE-m interact with each other, the water entropy increases and therefore, escalates the randomness of the association between adsorbate and adsorbent, allowing both pigmented compounds to diffuse through the boundary layer to reach the surface of RSE-m which is covered by the hydrophobic tail of CTAB.
- As both RSE-m and pigmented compounds share similar hydrophobicity, the adsorption of carotenoids is mainly caused by the physical hydrophobic binding, while it is driven by hydrophobic and electrostatic interactions for chlorophyll (as illustrated in Fig. 8).

4. Conclusions

RSE-m has been successfully employed as an adsorbent to reduce the impurities of glycerol, including FFA, carotenoids, and chlorophyll. The highest removal rate of the three impurities is obtained at $T = 40$ °C, $m_h = 15$, and $m_c = 0.75$ wt%. Both adsorption temperature and RSE-m loading show significant influence on the removal of FFA and the pigmented compounds, with the maximum removal rate, is observed at the adsorption condition of $T_a = 50$ °C, $t = 60$ min, and $m_a = 10$ wt%. RSE-m possesses a high affinity to both carotenoids and chlorophyll, reaching more than 93% removal rate. The resulting glycerol exhibits comparable specifications to the industrial-grade glycerol. The adsorption process is endothermic, spontaneous, and is governed by physisorption via hydrophobic binding (for both pigmented compounds) and electrostatic

Table 6
Isotherm parameters of the adsorption of pigmented compounds onto RSE-m.

Isotherm	Parameters	Temperature (K)					
		Carotenoids			Chlorophyll		
		303	323	343	303	323	343
Langmuir	$Q_{m(L)}$ (mg/g)	804.69	850.51	844.80	64.04	67.68	67.70
	K_L (L/mg)	0.17	0.21	0.20	1.85	2.48	2.61
	r^2	0.9880	0.9586	0.9891	0.9617	0.9736	0.9823
Freundlich	K_F ((mg/g) (L/mg)$^{1/n}$)	138.62	151.68	149.83	50.15	53.33	58.36
	1/n	0.59	0.62	0.61	0.61	0.62	0.65
	r^2	0.9617	0.9245	0.9758	0.9332	0.9396	0.9683
Dubinin-Radushkevich	$Q_{m(D-R)}$ (mg/g)	468.70	483.92	471.16	45.71	47.13	49.31
	E (kJ/mol)	0.92	1.04	1.16	3.41	3.93	4.31
	r^2	0.9364	0.9422	0.9131	0.9695	0.9801	0.9696

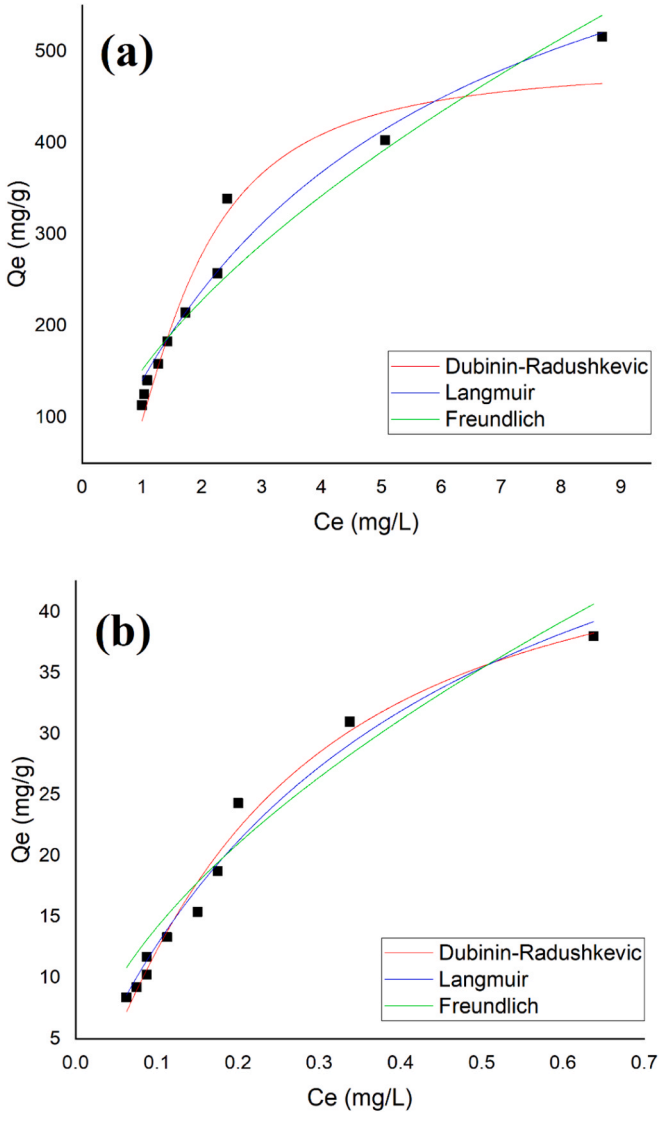

Fig. 7. The isotherm profiles for the adsorption of (a) carotenoids and (b) chlorophyll to RSE-m surface (T_a = 50 °C, t = 60 min, agitation speed = 300 rpm).

Table 7
Thermodynamic parameters of the adsorption of carotenoids and chlorophyll onto the surface of RSE-m.

Temperature (K)	Thermodynamic parameters					
	Carotenoids			Chlorophyll		
	ΔG° (kJ/mol)	ΔH° (kJ/mol)	ΔS° (J/mol.K)	ΔG° (kJ/mol)	ΔH° (kJ/mol)	ΔS° (J/mol.K)
353	−28.77	3.399	106.5	−36.07	7.336	143.6
373	−31.24			−39.24		
393	−33.03			−41.81		

interaction (for chlorophyll only).

CRediT authorship contribution statement

Maria Yuliana: Conceptualization, Methodology, Investigation, Software, Writing, Resources. **Luciana Trisna:** Investigation, Software, Validation. **Feprita Sari:** Investigation, Validation. **Valentino Bervia Lunardi:** Software, Visualization.

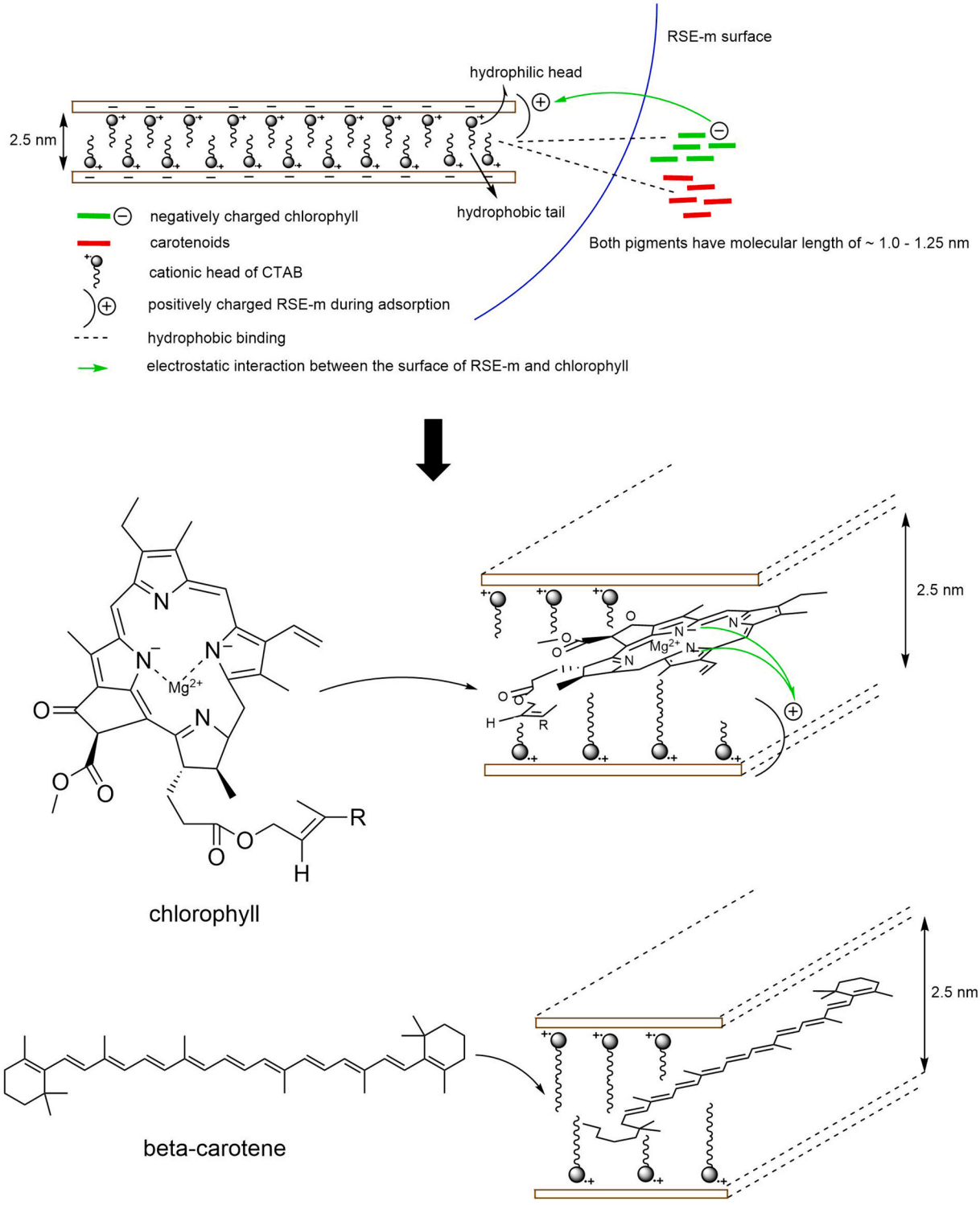

Fig. 8. The schematic interaction between the pigmented compounds and the surface of RSE-m.

Declaration of Competing Interest

The authors declare that they have no known competing financial interests or personal relationships that could have appeared to influence the work reported in this paper.

Acknowledgement

The authors would like to thank PT. BEST, a local biodiesel manufacturer in Indonesia, for assistance in the preliminary sample and data collection.

References

[1] M.R. Monteiro, C.L. Kugelmeier, R.S. Pinheiro, M.O. Batalha, A. da Silva César, Glycerol from biodiesel production: technological paths for sustainability, Renew. Sustain. Energy Rev. 88 (2018) 109–122, https://doi.org/10.1016/j.rser.2018.02.019.
[2] Menteri Energi dan Sumber Daya Mineral Republik Indonesia, SK Pengadaan BBN PSO Periode Mei - Desember 2018 FINAL.pdf, Jakarta, 2020.
[3] A. Talebian-Kiakalaieh, N.A.S. Amin, H. Mazaheri, A review on novel processes of biodiesel production from waste cooking oil, Appl. Energy 104 (2013) 683–710, https://doi.org/10.1016/j.apenergy.2012.11.061.
[4] M. Hasheminejad, M. Tabatabaei, Y. Mansourpanah, M.K. far, A. Javani, Upstream and downstream strategies to economize biodiesel production, Bioresour. Technol. 102 (2011) 461–468, https://doi.org/10.1016/j.biortech.2010.09.094.
[5] D. Samul, K. Leja, W. Grajek, Impurities of crude glycerol and their effect on metabolite production, Ann. Microbiol. 64 (2014) 891–898, https://doi.org/10.1007/s13213-013-0767-x.
[6] A.A. Abdul Raman, H.W. Tan, A. Buthiyappan, Two-step purification of glycerol as a value added by product from the biodiesel production process, Front. Chem. 7 (2019) 1–9, https://doi.org/10.3389/fchem.2019.00774.
[7] V. Razaviarani, I.D. Buchanan, S. Malik, H. Katalambula, Pilot scale anaerobic co-digestion of municipal wastewater sludge with biodiesel waste glycerin, Bioresour. Technol. 133 (2013) 206–212, https://doi.org/10.1016/j.biortech.2013.01.101.
[8] J.M. Fonseca, J.G. Teleken, V. de Cinque Almeida, C. da Silva, Biodiesel from waste frying oils: methods of production and purification, Energy Convers. Manag. 184 (2019) 205–218, https://doi.org/10.1016/j.enconman.2019.01.061.
[9] F.D. Santos, L.R.V. da Conceição, A. Ceron, H.F. de Castro, Chamotte clay as potential low cost adsorbent to be used in the palm kernel biodiesel purification, Appl. Clay Sci. 149 (2017) 41–50, https://doi.org/10.1016/j.clay.2017.09.009.
[10] N.Z. binti K. Shaari , T.L. Ooi , N.S.M. binti N.M. Din , S. Ahmad , Process for reducing color ofa polyglycerol, US8404904B2, 2013.
[11] B. Kocak, S. Yapar, Bleaching of crude glycerol by organobentonite, Gazi Univ. J. Sci. 24 (2011) 867–876.
[12] I. Mukherjee, B.K. Sovacool, Palm oil-based biofuels and sustainability in southeast Asia: a review of Indonesia, Malaysia, and Thailand, Renew. Sustain. Energy Rev. 37 (2014) 1–12, https://doi.org/10.1016/j.rser.2014.05.001.
[13] J.I. Chang, H.S. Tai, T.H. Huang, Regeneration of spent bleaching earth by lye-extraction, Environ. Prog. 25 (2006) 373–378, https://doi.org/10.1002/ep.10170.
[14] S. Zhu, M. Xia, Y. Chu, M.A. Khan, W. Lei, F. Wang, T. Muhmood, A. Wang, Adsorption and desorption of Pb(II) on L-Lysine modified montmorillonite and the simulation of interlayer structure, Appl. Clay Sci. 169 (2019) 40–47, https://doi.org/10.1016/j.clay.2018.12.017.
[15] S. Zhu, M. Asim Khan, F. Wang, Z. Bano, M. Xia, Rapid removal of toxic metals Cu2 + and Pb2+ by amino trimethylene phosphonic acid intercalated layered double hydroxide: a combined experimental and DFT study, Chem. Eng. J. 392 (2020), 123711, https://doi.org/10.1016/j.cej.2019.123711.
[16] S.P. Santoso, A.E. Angkawijaya, M. Yuliana, V. Bundjaja, F.E. Soetaredjo, S. Ismadji, A.W. Go, P.L. Tran-Nguyen, A. Kurniawan, Y.H. Ju, Saponin-intercalated organoclays for adsorptive removal of β-carotene: equilibrium, reusability, and phytotoxicity assessment, J. Taiwan Inst. Chem. Eng. 117 (2020) 198–208, https://doi.org/10.1016/j.jtice.2020.11.036.
[17] R.S. Pohndorf, T.R.S. Cadaval, L.A.A. Pinto, Kinetics and thermodynamics adsorption of carotenoids and chlorophylls in rice bran oil bleaching, J. Food Eng. 185 (2016) 9–16, https://doi.org/10.1016/j.jfoodeng.2016.03.028.
[18] Y.T. Khok, C.H. Ooi, A. Matsumoto, F.Y. Yeoh, Reactivation of spent activated carbon for glycerine purification, Adsorption 26 (2020) 1015–1025, https://doi.org/10.1007/s10450-020-00210-x.
[19] A. Gürses, K. Güneş, F. Mindivan, M.E. Korucu, M. Açikyildiz, Ç. Doıar, The investigation of electrokinetic behaviour of micro-particles produced by CTA + ions and Na-montmorillonite, Appl. Surf. Sci. 318 (2014) 79–84, https://doi.org/10.1016/j.apsusc.2014.01.036.
[20] M.J. Rosen, Relationship of structure to properties in surfactants. III. Adsorption at the solid-liquid interface from aqueous solution, J. Am. Oil Chem. Soc. 52 (1975) 431–435, https://doi.org/10.1007/BF02637482.
[21] M. Yuliana, R.J. Sutrisno, S. Hermanto, S. Ismadji, C.J. Wijaya, S.P. Santoso, F. E. Soetaredjo, Y.H. Ju, Hydrophobic cetyltrimethylammonium bromide-pillared bentonite as an effective palm oil bleaching agent, ACS Omega 5 (2020) 28844–28855, https://doi.org/10.1021/acsomega.0c04238.
[22] A. Kurniawan, H. Sutiono, Y.H. Ju, F.E. Soetaredjo, A. Ayucitra, A. Yudha, S. Ismadji, Utilization of rarasaponin natural surfactant for organo-bentonite preparation: application for methylene blue removal from aqueous effluent, Microporous Mesoporous Mater. 142 (2011) 184–193, https://doi.org/10.1016/j.micromeso.2010.11.032.
[23] A.M. Motawie, M.M. Madany, A.Z. El-Dakrory, H.M. Osman, E.A. Ismail, M. M. Badr, D.A. El-Komy, D.E. Abulyazied, Physico-chemical characteristics of nano-organo bentonite prepared using different organo-modifiers, Egypt. J. Pet. 23 (2014) 331–338, https://doi.org/10.1016/j.ejpe.2014.08.009.
[24] D.S. Moraes, L.C.R. Miranda, R.S. Angélica, G.N. Rocha Filho, J.R. Zamian, Functionalization of bentonite and vermiculite after the creation of structural defects through an acid leaching process, J. Braz. Chem. Soc. 29 (2018) 320–327, https://doi.org/10.21577/0103-5053.20170143.
[25] A. dos Santos, M.F. Viante, D.J. Pochapski, A.J. Downs, C.A.P. Almeida, Enhanced removal of p-nitrophenol from aqueous media by montmorillonite clay modified with a cationic surfactant, J. Hazard. Mater. 355 (2018) 136–144, https://doi.org/10.1016/j.jhazmat.2018.02.041.
[26] Z. Wu, T. Shang, Y. Deng, Y. Tao, Q.H. Yang, The assembly of MXenes from 2D to 3D, Adv. Sci. 7 (2020), 1903077, https://doi.org/10.1002/advs.201903077.
[27] M. Chigondo, H.K. Paumo, M. Bhaumik, K. Pillay, A. Maity, Magnetic arginine-functionalized polypyrrole with improved and selective chromium(VI) ions removal from water, J. Mol. Liq. 275 (2019) 778–791, https://doi.org/10.1016/j.molliq.2018.11.032.
[28] H.J. Lee, H.S. Lee, J. Seo, Y.H. Kang, W. Kim, T.H.K. Kang, State-of-the-art of cellulose nanocrystals and optimal method for their dispersion for construction-related applications, Appl. Sci. 9 (2019) 1–14, https://doi.org/10.3390/app9030426.
[29] S. Chowdhury, R. Mishra, P. Saha, P. Kushwaha, Adsorption thermodynamics, kinetics and isosteric heat of adsorption of malachite green onto chemically modified rice husk, Desalination 265 (2011) 159–168, https://doi.org/10.1016/j.desal.2010.07.047.
[30] H. More, Factors Affecting Adsorption, 2018.
[31] SRS Engineering Corporation, Glycerin Specifications, 2013. http://www.srsbiodiesel.com/technologies/glycerin-purification/glycerin-specifications/.(Accessed 28 November 2020).
[32] M. Hunsom, C. Autthanit, Adsorptive purification of crude glycerol by sewage sludge-derived activated carbon prepared by chemical activation with H3PO4, K2CO3 and KOH, Chem. Eng. J. 229 (2013) 334–343, https://doi.org/10.1016/j.cej.2013.05.120.
[33] M.A. Simon, E. Anggraeni, F.E. Soetaredjo, S.P. Santoso, W. Irawaty, T.C. Thanh, S. B. Hartono, M. Yuliana, S. Ismadji, Hydrothermal synthesize of HF-Free MIL-100 (Fe) for isoniazid-drug delivery, Sci. Rep. 9 (2019) 1–11, https://doi.org/10.1038/s41598-019-53436-3.
[34] Y.S. Ho, G. McKay, Pseudo-second order model for sorption processes, Process Biochem. 34 (1999) 451–465.
[35] L. Widdyaningsih, A. Setiawan, S.P. Santoso, F.E. Soetaredjo, S. Ismadji, S. B. Hartono, Y.H. Ju, P.L. Tran-Nguyen, M. Yuliana, Feasibility study of nanocrystalline cellulose as adsorbent of steryl glucosides from palm-based biodiesel, Renew. Energy 154 (2020) 99–106, https://doi.org/10.1016/j.renene.2020.03.001.
[36] C.S. Zhu, L.P. Wang, W. bin Chen, Removal of Cu(II) from aqueous solution by agricultural by-product: peanut hull, J. Hazard. Mater. 168 (2009) 739–746, https://doi.org/10.1016/j.jhazmat.2009.02.085.
[37] Q. Li, L. Chai, Z. Yang, Q. Wang, Kinetics and thermodynamics of Pb(II) adsorption onto modified spent grain from aqueous solutions, Appl. Surf. Sci. 255 (2009) 4298–4303, https://doi.org/10.1016/j.apsusc.2008.11.024.
[38] Y. Liu, Y.J. Liu, Biosorption isotherms, kinetics and thermodynamics, Sep. Purif. Technol. 61 (2008) 229–242, https://doi.org/10.1016/j.seppur.2007.10.002.
[39] M.H. Baik, S.Y. Lee, Colloidal stability of bentonite clay considering surface charge properties as a function of pH and ionic strength, J. Ind. Eng. Chem. 16 (2010) 837–841, https://doi.org/10.1016/j.jiec.2010.05.002.
[40] R.D. Gougeon, M. Reinholdt, L. Delmotte, J. Miehé-Brendlé, J.M. Chézeau, R. Le Dred, R. Marchal, P. Jeandet, Direct observation of polylysine side-chain interaction with smectites interlayer surfaces through 1H-27al heteronuclear correlation NMR spectroscopy, Langmuir 18 (2002) 3396–3398, https://doi.org/10.1021/la0115381.
[41] P. Liu, M. Du, P. Clode, H. Li, J. Liu, Y.K. Leong, Surface chemisty, microstructure, and rheology of thixotropic 1-D sepiolite gels, Clays Clay Min. 68 (2020) 9–22, https://doi.org/10.1007/s42860-019-00050-z.